PCCP

PAPER

View Article Online
View Journal | View Issue

Cite this: *Phys. Chem. Chem. Phys.*, 2014, **16**, 14834

High resolution NEXAFS of perylene and PTCDI: a surface science approach to molecular orbital analysis†

Guido Fratesi,[a] Valeria Lanzilotto,[bd] Stefano Stranges,[cd] Michele Alagia,[d] Gian Paolo Brivio[e] and Luca Floreano*[d]

Received 15th April 2014,
Accepted 4th June 2014

DOI: 10.1039/c4cp01625d

www.rsc.org/pccp

We made use of synchrotron radiation to perform near edge X-ray absorption fine structure spectroscopy, NEXAFS, at the carbon K-edge of perylene and perylene-tetracarboxylic-diimide, PTCDI. Reference spectra measured for isolated molecules in the gas phase are compared with polarization dependent NEXAFS spectra measured on highly oriented thin films in order to study the symmetry of the molecular orbitals. The molecular overlayers are grown onto the rutile TiO_2(110) surface for which the large anisotropic corrugation effectively drives the molecular orientation, while its dielectric nature prevents the rehybridization of the molecular orbitals. We employed density functional theory, DFT, calculations to disentangle the contribution of specific carbon atoms to the molecular density of states. Numerical simulations correctly predict the observed NEXAFS azimuthal dichroism of the σ* resonances above the ionization threshold, from which we determine the full geometric orientation of the overlayer molecules. A discrepancy observed for the spectral contribution of the imide carbon atom to the calculated unoccupied molecular orbitals has been explained in terms of initial state effects, as determined by Hartree–Fock corrections and in full agreement with the corresponding shift of the C 1s core level measured by X-ray photoelectron spectroscopy, XPS.

1 Introduction

Polycyclic aromatic hydrocarbons, PAHs, represent a class of molecular semiconductors that are widely employed in electronic devices spanning from solar cells to plastic electronics thanks to their thermal stability and flexible processing protocols. Among them, perylene, $C_{20}H_{12}$, a planar molecule with D_{2h} symmetry displaying a dominant electron–donor character (p-type semiconductor), is the basis for the synthesis of multiple derivatives thanks to the possibility to functionalize the molecule in its different peripheral terminations.

Much effort in the past has been devoted to the investigation of the fundamental properties of perylene-tetra-carboxylic-dianhydride, PTCDA,[1,2] which is relevant for the realization of dye-sensitized[3] and donor–acceptor[4] organic photovoltaic, OPV, devices, as well as organic field effect transistors, OFETs.[5] More recently, a new class of n-type organic semiconductors, based on PTCDI derivatives, has been demonstrated capable of filling the historical gap between p-type and n-type OFETs in terms of both charge mobility and environmental stability.[6,7]

Ahead of an impressive increase of the number of newly synthesized PTCDI derivatives for both OPVs[8] and OFETs,[9] the advanced modeling of perylenes is mostly focused on the intermolecular coupling geometry,[10] which affects the optical spectrum,[11] and on the structure of monolayer phases at surfaces.[12–14] From the experimental point of view, the spectroscopic characterization of the molecular orbitals of the free PTCDI molecule, as well as of perylene, is largely outdated or limited.[15–18] In this context, the knowledge of the molecular orbital symmetry and energy, as measured in NEXAFS, is fundamental to understand the key parameters that govern the performances of an archetypal device, such as the orientation of the molecules on the surfaces[19] and the mechanism of charge transfer to the substrate.[20] In their extended review, Zahn and coworkers reported a comparative study of the electronic and vibrational properties of PTCDA and dimethyl-PTCDI,[2] however their analysis of NEXAFS spectra was limited to the comparison with previous calculations for naphthalene-tetracarboxylic

[a] *Dipartimento di Fisica, Università degli Studi di Milano, Via Celoria 16, I-20133 Milano, Italy*
[b] *Dipartimento di Chimica, Università degli Studi di Firenze, Via della Lastruccia 3, I-50019 Sesto Fiorentino, Italy*
[c] *Dipartimento di Chimica e Tecnologia del Farmaco, Università degli Studi di Roma "La Sapienza", Roma, Italy*
[d] *CNR-IOM, Laboratorio TASC, Km 163.5, Basovizza SS-14, I-34149 Trieste, Italy. E-mail: floreano@iom.cnr.it*
[e] *ETSF, CNISM, Dipartimento di Scienza dei Materiali, Università di Milano-Bicocca, via Cozzi 53, 20125 Milano, Italy*

† Electronic supplementary information (ESI) available. See DOI: 10.1039/c4cp01625d

dianhydride (NTCDA),[21] thus a clearcut disentanglement between initial and final state effects in the PTCDI NEXAFS is still missing.

In recent years, the NEXAFS simulation codes have been applied to an increasing number of aromatic systems computed *via* density functional theory, DFT, most often within the transition-potential method,[22] where the electronic structure is computed in the presence of a half core hole, HCH, at the excited atom. The good agreement with measured spectra[23–26] justifies the use of these models for the interpretation of experimental data, as compared to a quantum chemistry approach.[27] The experimental spectra measured in the gas phase can be simulated with excellent agreement by including specific corrections to the NEXAFS computations for addressing fine details such as the coupling to vibrational states.[28] Time dependent DFT calculations have been successfully extended to treat also core level excitations in heterocyclic aromatics.[29] On the other hand, the renovated interest in NEXAFS simulations of poly- and heterocyclic aromatics is associated with the study of their interaction with substrates of technological interest. In this context, the relevant parameters for understanding the molecule to substrate interaction from NEXAFS measurements are the atom resolved contributions to the absorption spectra and the electronic structure of the unoccupied molecular orbitals, MOs, in the presence of the core–hole.[25,26] The inclusion of a realistic model of the substrate into an *ab initio* calculation renders the implementation of most sophisticated corrections difficult or unfeasible due to the computational cost to treat the coupled system. Thus, it becomes important to understand the reliability extent of the consolidated DFT approaches for which such calculations are more accessible.

Hereafter we present a combined experimental and theoretical description of the unoccupied molecular orbitals for perylene and PTCDI. We compare NEXAFS spectra measured in the gas phase with polarization dependent NEXAFS measured on highly oriented thin films in order to identify the symmetry of the molecular orbitals. With the support of this experimental evidence, the comparison with DFT simulations performed in the half core–hole, HCH, approximation[25] allowed us to disentangle unequivocally the atom specific contributions in the NEXAFS resonances beyond the initial state effect. To this purpose, we have exploited the templating properties of the rutile $TiO_2(110)$ surface. The large anisotropic corrugation of this substrate is known to steer the orientation of planar D_{2h} symmetry aromatic molecules, such as tetracene,[30] pentacene,[31] PTCDI[32] and PTCDA.[14] A common feature of these films in the monolayer range is the accommodation of the molecules with their major axis oriented along the substrate [001] direction, and slightly tilted around the major axis in order to fit the substrate spacing, eventually allowing for intermolecular π–π coupling.[31–33] This geometry can be preserved for a few layers displaying a good π-stacking, as reported for pentacene[31] and PTCDI.[32] Our DFT models are readily applicable to the condensed phases of poly- and heteroaromatics on $TiO_2(110)$ with the perspective of describing also the possible charge transfer and interaction with the oxygen vacancies that make the reduced surfaces of titania conductive and chemically reactive.

2 Experimental and theoretical methods

2.1 Experimental details

Absorption and photoemission spectroscopy measurements have been performed at the gas phase and ALOISA beamlines of the Elettra Synchrotron (Trieste, Italy). Gas phase NEXAFS spectra have been measured at the ARPES end station[34] by recording the total ion yield using a channeltron with the photon energy resolution set to 30 meV. PTCDI and perylene molecular beams were produced using a resistively heated stainless steel furnace internally lined with boron nitride in order to prevent molecular decomposition at the metal walls of the crucible. The absolute photon energy has been calibrated in real time by letting in CO traces during NEXAFS acquisition. For comparison, reference NEXAFS spectra in the solid state have been measured at ALOISA on thin films (up to ∼15 Å, as determined by quartz microbalance calibration) grown on the $TiO_2(110)$ surface by organic molecular beam deposition (boron nitride crucible).

In the case of perylene, we observed by XPS the saturation of the first layer (hereafter defined as 1 monolayer) at an equivalent thickness of ∼3.0 Å for deposition at room temperature, RT, at a rate of ∼0.1 Å min^{-1}. This might be due to the very high mobility of perylene, which would form very widely spaced 3D clusters, as reported for Cu(110),[35] thus escaping detection by surface sensitive large area probes, such as XPS, at the overall small thickness considered here. As an alternative, we cannot exclude a reduced sticking associated with a molecular arrangement of the first layer that would impair the building up of the native crystal phase. Upon cooling the sample at 200 K, we observed by XPS the condensation of further layers, which however grow in a tilted-up orientation. A part from the degree of order and molecular orientation, we have observed no variations between the electronic structure of the room temperature monolayer phase and a low temperature multilayer film, in full agreement with former observations for the similar case of pentacene, where the monolayer phase was found to reproduce the NEXAFS of its bulk phase down to the tiniest spectral feature.[31] For the present perylene study of the molecular orbital symmetry, we thus used the highly oriented monolayer phase at room temperature.

A priori, the substrate interaction may be stronger in the case of functionalized molecules such as PTCDI. In particular, the UHV preparation of the $TiO_2(110)$ (Ar^+ ion bombardment followed by flash to ∼1000–1050 K) is known to yield a slightly reduced surface with a concentration of a few percent of oxygen vacancies, O_{vac}. The latter ones are associated with a redistribution of electrons on the Ti lattice sites that makes the surface conductive and reactive.[36,37] In this regard, an interaction of the imide termination of PTCDI with the O_{vac} cannot be excluded, since pyridine derivatives have been reported to display a preferential adsorption at oxygen vacancies.[38,39] A direct comparison of the PTCDI NEXAFS spectra for a monolayer and a multilayer on $TiO_2(110)$ reveals small differences in the relative intensity of the LUMO fine structures,[32] which

might be associated with a minority of molecules interacting with the substrate O_{vac}. For this reason, we considered the NEXAFS spectra of the multilayer PTCDI film for the comparison with the gas phase data. In this way, we get rid of unwanted contributions from PTCDI molecules interacting with the oxygen vacancies, while the film still displays a strong anisotropic preferential orientation of the molecules, which is much useful for the study of the molecular orbital symmetry. The NEXAFS spectra of the PTCDI multilayer on TiO_2 are reported in ref. 32, which nominal thickness of 15 Å corresponds to 5 equivalent layers of molecules with the same planar stacking geometry of the first layer.

NEXAFS spectra taken with linearly polarized radiation on these highly oriented films display a pronounced dichroism when taken in the two opposite polarizations, *i.e.* in Transverse Magnetic, TM, and Transverse Electric, TE, geometry, as referred to the scattering plane, thus allowing us to discriminate between π and σ symmetry resonances. At the ALOISA end-station, the spectra have been taken at a constant grazing angle of 6° by rotating the sample around the photon beam axis without changing the beam footprint on the surface, so that the TE geometry corresponds to s-polarization and TM geometry is close to p-polarization (see Fig. 1 in ref. 40 for a sketch of the scattering geometry). Eventually, TE spectra have been measured for different surface azimuthal orientations. The spectra were taken in partial electron yield and the absolute energy calibration was performed a posteriori through the characteristic signal of the C K-edge in the reference drain current, as simultaneously measured on the last mirror optics. The discrepancy between the two different calibration procedures at the gas phase and ALOISA beamlines is within 0.1 eV. The spectra at ALOISA have been recorded with an energy resolution of ~70 meV and with a bias of −250 volt applied to a grid in front of the detector (channeltron) in order to reject the tail of the secondary electrons.

The XPS spectra of C 1s have also been measured on the molecular films at a photon energy of 650 eV with an overall energy resolution of ~270 meV. We have calibrated the energy scale of the XPS spectra to the substrate Ti $2p_{3/2}$ peak at 459.1 eV, from which the characteristic defect state in the gap of the TiO_2(110) surface results to be located at a binding energy of ~0.9 eV. Perylene and PTCDI powders (declared purity 98%) were purchased by Alfa Aesar (ref. L03047 and 44098, respectively) and used as received. Both the furnace (gas phase beamline) and the crucible (ALOISA beamline) were operated at typical temperatures of 390–400 K and 680–690 K for perylene and PTCDI, respectively.

2.2 Computational details

Numerical simulations based on DFT were run for isolated molecules in periodically repeated supercells, with pseudopotentials and the plane-wave basis set, as implemented in the Quantum-Espresso distribution.[41] The theoretical method and the numerical setup are the same as in our previous work,[25] which is referred to for details while the main points are summarized next. We used the Perdew Burke Ernzerhof (PBE)[42] generalized gradient approximation to the exchange and correlation functional. Molecules were placed in orthorhombic supercells with 11 Å of vacuum space between replicas. Geometry optimization was performed for the neutral molecules. Total energy calculations at fixed coordinates with a C pseudopotential generated with a 1s full core hole (FCH)[43] at a given atom site were used to evaluate core level shifts between inequivalent carbon atoms as relevant for XPS and the NEXAFS initial state. We considered the individual contributions to the spectra by the six (seven) inequivalent carbon atoms for perylene (PTCDI), according to the labeling in Fig. 1, as taken from ref. 2. Eventually, the hybrid functional PBE0,[44] which includes a fraction of Hartree–Fock exchange, was also used to compute the core shifts. The transition-potential calculation of NEXAFS spectra for the excitation of each inequivalent C atom in the molecule was performed by the xspectra code,[45] based on a self-consistent calculation of the effective potential with half-core–hole (HCH) pseudopotential at that site.[22,46] This setup allows us to estimate efficiently the spectrum also in the continuum energy region, which is especially relevant to determine the azimuthal orientation of the molecules.[25] We notice that transition-potential

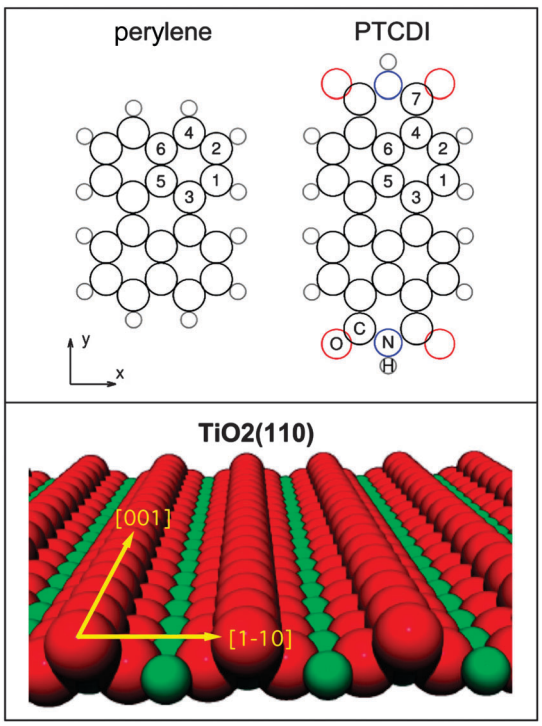

Fig. 1 Top panel: sketch of the perylene and PTCDI atomic structure with the labeling of carbon atoms, as adopted hereafter. The imide carbon atoms are labeled C7, while C4, C2 and C1 correspond to the pery-, ortho- and bay-positions, respectively. The inner carbon atoms C5 and C6 have a double multiplicity, whereas all of the other carbon atoms display a quadruple multiplicity. Bottom panel: perspective view of the rutile TiO_2(110) surface with large (red) and small (green) balls representing O and Ti atoms, respectively. The rows of bridge-oxygen atoms running along the [001] direction protrude ~1–1.2 Å out of the first Ti plane (according to XRD[47] and LEED *I*–*V*[48] measurements). Adjacent bridge-oxygen rows are spaced by 6.495 Å, and the bridge-oxygen atoms are spaced by 2.959 Å along the rows.

results can be further improved by considering explicitly the individual transitions.[26] However, this is only possible for the discrete part of the spectrum, thus excluding resonances in coupled systems or above the ionization threshold. Finally, by using a pseudopotential approach, the XPS and NEXAFS spectra of the molecule are both defined up to an energy constant, which will be adjusted in the following to match the most prominent feature with the experimental one.

As the use of plane-wave basis sets is relatively uncommon for the simulation of gas-phase NEXAFS spectra, it is worth highlighting that our approach has provided results in very good agreement with experiments for other PAHs like pentacene[25,31] and anthracene,[25,26] similarly to earlier calculations with the localized basis set.[26,49] In particular, detailed coincidence between plane-wave results[25] and localized-basis set (with diffuse functions) ones[26] for anthracene clearly demonstrates that the basis set can be freely chosen. Plane-wave basis sets are possibly more easily extended to the explicit inclusion of the substrate.

3 Results and discussion

3.1 Core level photoemission

The C 1s photoemission spectrum of the perylene monolayer is characterized by a single broad peak centered at 284.60 eV binding energy (upper panel of Fig. 2), where the different contributions of the inequivalent carbon atoms are unresolved, even if the peak is clearly skewed toward lower energies. A well defined satellite peak is also observed at 1.85 ± 0.05 eV higher binding energy, which is associated with the energy loss corresponding to the excitation by the C 1s photoelectrons of an HOMO–LUMO transition (shake-up satellite), in full agreement with previous reports on analogous PAHs.[50] The C 1s spectra of the PTCDI multilayer is quite similar to the perylene one (lower panel of Fig. 2) displaying a main peak centered at 285.06 eV binding energy. The main spectral feature of PTCDI is shifted by ~0.45 eV toward higher binding energy because of the overall charge withdrawal from the perylene core due to the imide groups, whose carbon peak is located at 3.15 eV higher binding energy. The latter value compares well with the core-level shifts (CLSs) of 3.04 eV and 3.1 eV reported for dimethyl-PTCDI[2] and ethylpropyl-PTCDI,[51] respectively, where the additional functionalization of the imide termination can be responsible for the residual difference with respect to the bare PTCDI. Finally, the peak of the imide carbon atom is also accompanied by a shake-up satellite at 1.4 eV higher energy, which is as intense as that associated with the main peak of the perylene core (at 1.85 eV from the main peak). From a qualitative point of view, the C 1s spectrum of PTCDI is similar to the PTCDA one.[50]

We calculated by DFT the initial state (binding energy) of the inequivalent carbon atoms in the molecule, which is also necessary to disentangle the contribution of different carbon atoms to the NEXAFS resonances associated with the core electron excitations into the unoccupied molecular orbitals, MOs. We performed calculations with both PBE and PBE0 functionals. As can be seen in Table 1, very small differences result between the two computational approaches in the case of perylene. The PBE0 core levels are shifted by 10–30 meV with respect to the PBE ones, resulting in an increase of the spread among the different carbon components. The PBE0 binding energies are also reported on top of the XPS spectrum as vertical bars with height proportional to the number of equivalent carbon atoms. Due to the large number of inequivalent atoms, we did not attempt a multicomponent deconvolution (fitting) of

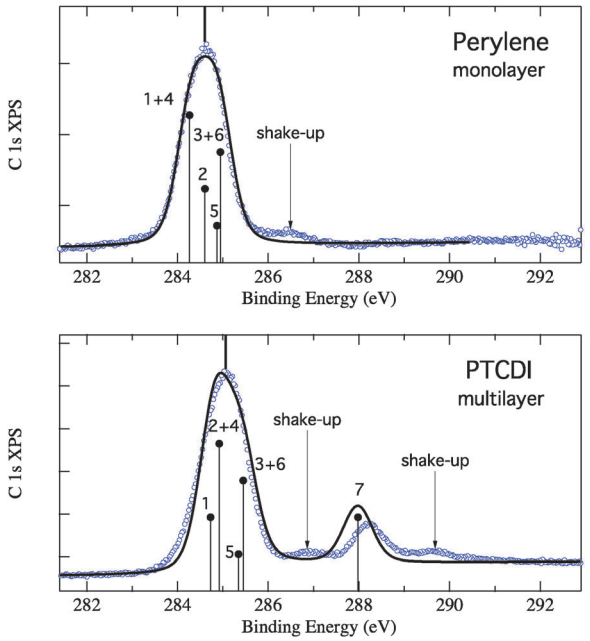

Fig. 2 The photoemission spectra of the C 1s core level recorded on a perylene monolayer and a PTCDI multilayer (~15 Å) grown on TiO_2(110) are shown as open markers in the upper and lower panels, respectively. The components of the inequivalent carbon atoms, as calculated by PBE0 functional, are superimposed as vertical bars according to the core level shifts reported in Table 1 with the same labeling. The core level shifts are relative to the average position of the main peak, *i.e.* 284.60 and 285.06 eV, for perylene and PTCDI, respectively, as indicated by the thick vertical bar. The height of each bar component is proportional to the corresponding number of equivalent atoms in the molecule. The full line is a simulation of the experimental spectrum obtained by associating each PBE0 component with a 0.2 eV wide Lorentzian peak convoluted with a 0.6 eV Gaussian broadening.

Table 1 Calculated core level shifts (in eV) with respect to the weighted average of the main peak (without C7) with PBE and PBE0 functionals. For comparison, we have also reported the experimental CLSs reported for DiMe-PTCDI[2] and PTCDA.[50] Our experimental estimate for the CLS of C7 in PTCDI is 3.15 eV

	Perylene		PTCDI		DiMe-PTCDI	PTCDA		
Atom	PBE	PBE0	PBE	PBE0	Exp.[2]	PBE	PBE0	Exp.[50]
C1 × 4	−0.30	−0.32	−0.30	−0.34	−0.36	−0.32	−0.36	0.188
C2 × 4	−0.01	0.01	−0.17	−0.14	−0.36	−0.17	−0.14	0.188
C3 × 4	0.34	0.35	0.36	0.38	0.34	0.35	0.37	−0.322
C4 × 4	−0.31	−0.34	−0.18	−0.22	0.04	−0.14	−0.18	0.268
C5 × 2	0.26	0.27	0.27	0.28	0.34	0.25	0.26	−0.322
C6 × 2	0.30	0.33	0.31	0.36	0.34	0.31	0.36	−0.322
C7 × 4	—	—	2.56	2.92	3.04	2.92	3.33	3.728

the experimental spectrum. However, a good simulation can be simply obtained by associating each PBE0 component with a Lorentzian peak convoluted with a Gaussian broadening. The simulation shown in Fig. 2 has been obtained by assuming a Lorentzian width of 0.2 eV and a Gaussian broadening of 0.6 eV without any further adjustment of the binding energy and the intensity ratio (as given by the simple atom multiplicity). The observed slight asymmetry of the experimental spectrum as well as the width of the Lorentzian contribution, which is found to be twice larger than the C 1s natural linewidth,[52,53] can be associated with the vibrational splitting of the single components that cannot be accounted for in our calculations.

When considering the PTCDI molecule, the components of the perylene core do not show significant variations, and the small displacements with respect to the average peak result into an overall slight increase of the peak spread, in full agreement with the observed broadening of the PTCDI main feature with respect to the perylene one. The difference between the PBE and PBE0 calculations becomes relevant for the carbon atom in the imide group, which is largely underestimated by the PBE functional, while the Hartree–Fock correction (PBE0) results into a smaller difference with the experimental result ($\sim$0.25 eV). In the next section, we will discuss in more detail how the simulated NEXAFS spectra are affected by the $\sim$0.6 eV energy difference between the PBE and the experimental imide carbon contribution.

When comparing with multicomponent fit analysis of PTCDI and derivatives,[2,51,54] we notice that DFT predicts the inequality between carbon atoms to be larger than previously envisaged. In particular, we find a significant difference of $\sim$0.5 eV between the carbon atom C4, linking the imide group (C–C type), and the other three types of C–C atoms, namely C3, C5, C6. This large core level shift is not due to the imide functionalization, since an even larger difference of $\sim$0.65 eV is found in perylene between the pery-carbon atom (C4) and the average of the C–C atoms (C3, C5, C6). Along with the same issue, we also find the two C–H atoms in ortho- (C2) and bay- (C1) positions to differ one from the other by $\sim$0.3 eV in perylene and $\sim$0.2 eV in PTCDI, whereas they are commonly assumed to display the same CLS.[2,51]

These results can be compared to those for PTCDA, as measured by Zahn and coworkers[2] and by Schöll and coworkers.[50] We first consider the carbon atom C7 of the anhydride group, which is experimentally found to be shifted at a much larger binding energy ($\sim$0.6 eV) with respect to that in the imide group. This effect is well reproduced by the PBE0 calculations, although the absolute CLS is underestimated in both perylene derivatives. Next, we focus on the C atoms of the perylene core. According to our calculations, the energy CLS of the carbon components in the perylene core of PTCDA does not differ from that of PTCDI within a few tens of meV, in full agreement with the fitting analysis of Zahn and coworkers, who found the same CLS for DiMe-PTCDI and PTCDA.[2] However, the assignment done in ref. 50, as reported in Table 1, is opposite to our values and we suggest that it is revised according to our results.

3.2 Carbon K-edge NEXAFS

3.2.1 Perylene. We first compare the gas phase NEXAFS spectrum of perylene with the angularly averaged total contribution calculated with the PBE functional, as shown in the upper panel of Fig. 3. For a better comparison with DFT calculations, we have taken the most prominent feature at 285.5 eV as a reference for spectral alignment. As it will be shown, this peak corresponds to a π^* symmetry resonance that is mainly associated with a transition from the core level to the LUMO + 1 excited state. Such a resonance can be easily identified in the whole family of perylene derivatives. From the experimental point of view, our spectrum is consistent with former NEXAFS spectra measured on single crystals[15,17] and on multilayer films,[16] even if our higher resolution allows us to resolve clearly the fine structure of the LUMO (whose splitting was first resolved in the crystalline phase[15]) and higher energy resonances.

The comparison between theory and experiments for perylene points out an optimal agreement for the first two groups of states (excitations to the LUMO and LUMO + 1 states in the 284–286 eV region), whereas there is an increasing mismatch for the higher energy resonances that occur in a narrower energy range in the simulation with respect to experiments. Indeed Kohn–Sham eigenvalues (here at the PBE level) give only an approximate description of the excitations of the system. Nonetheless, the qualitative agreement still allows the fine analysis of the spectra which will be presented next.

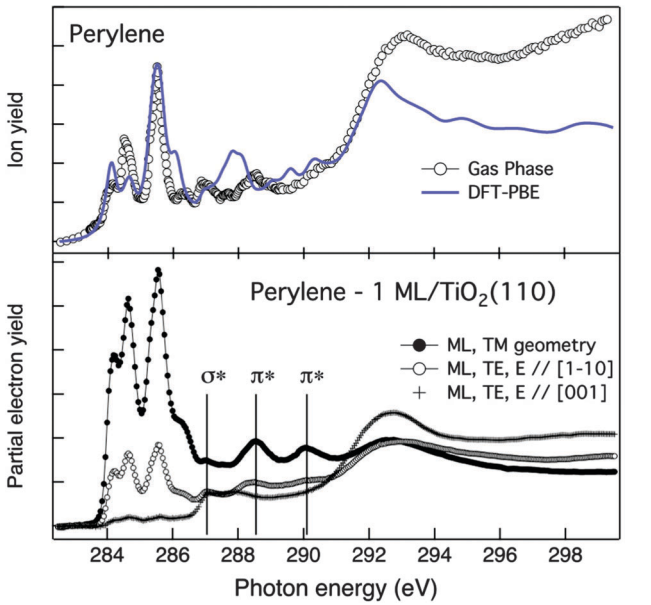

Fig. 3 Perylene NEXAFS. Upper panel: comparison between the gas phase NEXAFS spectrum and DFT–PBE simulation. The theoretical spectrum has been shifted by 289.18 eV, in order to match the most prominent and sharpest resonance at 285.5 eV. Lower panel: comparison between solid state spectra measured at different orientation of the surface with respect to the photon beam polarization. A direct comparison of the gas and condensed phase NEXAFS requires a shift of the gas phase spectrum by +0.07 eV. We attribute this small difference either to the discrepancy between the different calibration procedures or to minor polarization effects.

To disentangle the different atomic contribution to the excitations into the various unoccupied molecular orbitals and to analyze their symmetry, we take advantage of NEXAFS spectra measured on a highly oriented molecular layer. In this way, we can deal separately the core level transitions to molecular orbitals with different symmetry. By deposition on the surface held at room temperature, we formed a saturated monolayer of perylene on TiO_2(110). The electronic structure of the molecular orbitals is left unaffected by this dielectric substrate, whose interaction with the molecular overlayer is only of van der Waal's type, as previously reported.[18] We can observe in the lower panel of Fig. 3 a strong dichroism of the NEXAFS spectra taken in the two opposite polarizations (with the electric field either normal, TM, or parallel, TE, to the surface). Comparing the TE spectra taken with the electric field oriented along the two opposite surface symmetry directions, we observe also an azimuthal dichroism for the resonances at 284–286 eV and for the broad feature at ~293 eV. This indicates that molecules line up along the [001] surface direction, with a tilt of the molecular plane around the [001] direction. In this specific case, we can determine the tilt angle $\gamma \sim 26^\circ$ from the intensity ratio between the π* symmetry resonances taken in TE (with the electric field oriented transverse to the tilting axis) and TM geometry, following the relation $I_{TE,E//[1\bar{1}0]}/I_{TM} = \tan^2\gamma$, as appropriate for the given symmetries of the substrate rectangular lattice and of the π* orbitals.[19] With this homogeneous orientation of the molecules, the NEXAFS spectrum in TM geometry is dominated by the π* symmetry resonances, whereas almost exclusively σ* symmetry resonances can be detected in the TE spectrum measured with the electric field oriented in the molecular plane and along the substrate [001] direction, *i.e.* along the tilting molecular axis.

The symmetry of the main NEXAFS resonances in the gas phase spectrum can be unambiguously determined from the comparison of the TM and TE spectra, as labeled in the figure. In particular, we remark that several resonances in the 286–290 eV energy range are found to display a prevalent π* character, whereas the strong resonance at ~288.6 eV was previously associated with the σ* symmetry C–H bond.[17] As shown hereafter, transitions to such a C–H state contribute to the NEXAFS resonance at 287.1 eV, consistently with the experimentally observed dominant σ* character.

For a better assessment of the individual atomic contributions to the NEXAFS resonances, as well as of the corresponding unoccupied molecular orbitals, we calculated separately the NEXAFS spectral contributions of each carbon type (as indicated in Fig. 1). Since most of the lower-energy states displays a prevalent π* symmetry, we first analyze the PBE NEXAFS contribution perpendicular to the molecular plane (*Z* direction). This is compared in Fig. 4 with the experimental spectrum measured in TM geometry on the molecular layer. The first resonance is clearly associated with electron transitions localized on the carbon atoms in pery (C4) and bay (C1) positions. The second peak is associated in part with the remaining hydrogen-bound carbon atom C2 in the ortho position and, mainly, with a carbon atom from the inner ring (C3). The other two atoms only

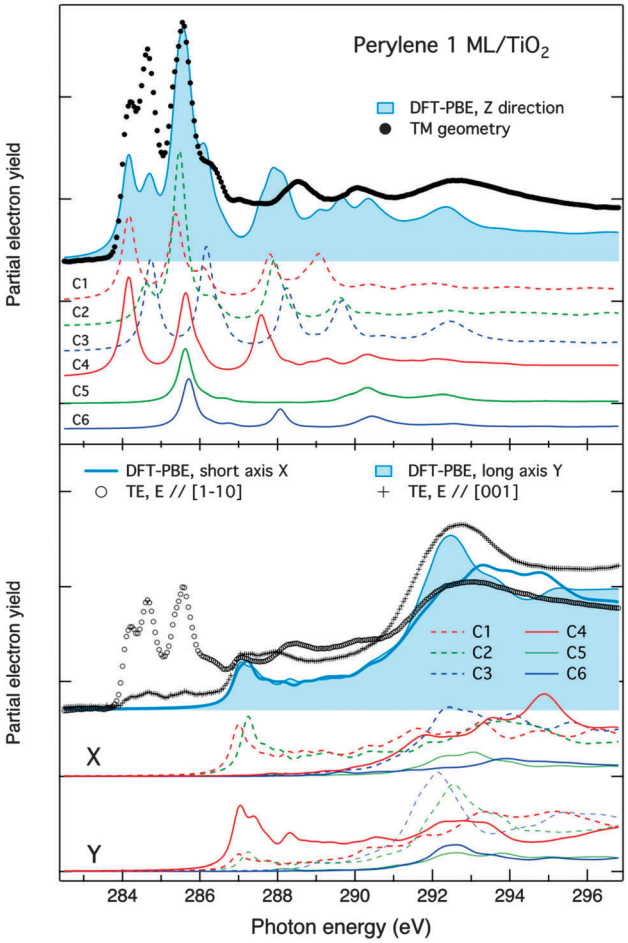

Fig. 4 Upper panel: comparison between perylene NEXAFS in the *z* direction (full shaded line) and a planar oriented molecular layer measured in TM geometry (filled markers). The atomically resolved contributions (weighted by the corresponding multiplicity) to the simulated NEXAFS are shown as dashed and full lines of different colors. Lower panel: comparison between perylene NEXAFS in the *XY* direction (shaded and full lines) and a planar oriented molecular layer measured in TE geometry (markers).

bound to carbon (C5, C6) do not contribute to the first two peaks. All atoms but C3 contribute to the third peak (the most prominent one), while the PBE calculated peak at 288 eV (which we associate with the experimental one observed at 288.6 eV) involves transitions starting from the 1s state of all the atoms but C5.

We now examine the contributions of the atomically localized 1s → LUMO + *i* transitions to the low-energy region of the spectrum. To this purpose, we recall that the spectrum can be approximated by the density of states at the ionized atom with the proper symmetry (see ref. 25 and ESI,† file), so it is convenient to analyze the (*i* + 1)th transition in terms of the valence state $|\Psi_{LUMO+i}\rangle$ (computed in the presence of the half core hole) and in particular of its projection on the $|2p_z\rangle$ atomic orbital at that atom, $|\langle\Psi|2p_z\rangle|^2$. Such squared overlap is reported in Fig. 5 for transitions up to the LUMO + 3. It is worth noticing that the localized core hole determines both initial and final state effects: it shifts the initial state energy

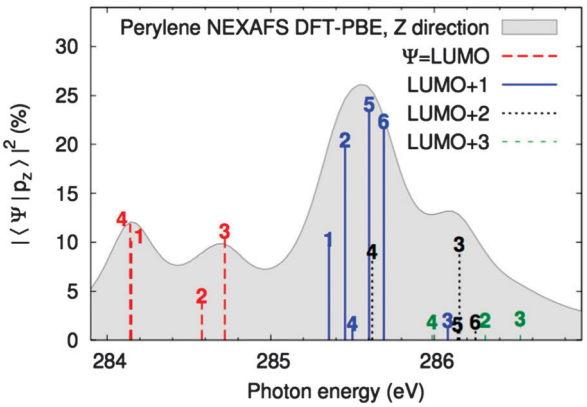

Fig. 5 The PBE calculated NEXAFS of perylene in the direction *Z* normal to the molecular plane (shaded curve) is shown together with vertical sticks representing the projection on the excited carbon atom $2p_z$ orbital (each stick is labeled by the number of the corresponding atom species) of the various unoccupied MOs, affected by the core hole.

(as seen in Table 1), and modifies the energy and wavefunction of the final-state orbitals (see the ESI† file for unoccupied MOs computed as a function of the position of the core hole). Our PBE calculations show that the LUMO of perylene is practically unaffected by these final state effects, wherever the core hole is created, while significant distortions are predicted for higher energy unoccupied MOs, where a rehybridization of the molecular orbitals of the neutral molecule can be observed. Coming back to Fig. 5, we clearly see that the first double peak is indeed due to transitions to LUMO states, and the splitting refers to the different CLS between C4/C1 and C3/C2. The inner carbon atoms C5 and C6 lie on the long molecular axis of perylene, which is a nodal plane for the LUMO, thus the 1s → LUMO transition is dipole-forbidden. The most prominent peak at ~285.5 eV is largely contributed by the LUMO + 1 resonances, but due to the orbital rehybridization it is also contributed by the LUMO + 2 resonance on atom C4. In general, we observe that the localized core hole significantly affects the spatial distribution and energy of the LUMO + *i* states, while the orbital nodal planes are more robust against rehybridization (see the ESI† file).

We now analyze the orbitals in the molecular plane. As can be seen in the lower panel of Fig. 4, the only resolved resonance below the ionization threshold is the aforementioned peak at 287.1 eV. This resonance is only contributed by the σ* resonance of the C–H bonds when the electric field is oriented parallel to the short molecular axis. An additional contribution from atom C4 arises when the electric filed is oriented parallel to the long axis. Most strikingly, we observe a large azimuthal dichroism of the broad σ* resonance at ~292.7 eV, above the ionization threshold, which shows a clear dependence on the photon electric field direction in the molecular plane. This allows us to determine the azimuthal orientation of perylene by comparison to the simulated spectra, like previously found for other uniaxial PAHs.[25] Here the energy position of the resonance peak does not change, but the intensity is remarkably higher in the [001] TE spectrum than in the [1$\bar{1}$0] one, whose behavior is well reproduced by comparing the PBE NEXAFS calculated along the major *Y* axis of the molecule with that along the short *X* axis, respectively. In the *Y* direction, the peak is mainly associated with excitations from core states localized onto C2 and C3 carbon atoms, but the contribution of the ortho carbon C2 is significantly reduced when the electric field is oriented along the short *X* axis. We can conclude that perylene in the monolayer is tilted around the long molecular axis, which is also aligned along the substrate [001] direction. We notice that the tilt angle of ~26° is rather small as compared with that of other poly- and heteroaromatics like PTCDI,[32] hexahydroxy-tri-phenylene[33] and pentacene[31] ($\gamma \sim 35°$, 32° and 25°, respectively). While still compatible with a molecular width slightly larger than 7 Å, this tilt angle would suggest that the perylene assembling is not driven by intermolecular π–π interaction, at variance with the aforementioned systems, rather it simply reflects the substrate corrugation.

3.2.2 PTCDI. The measured NEXAFS spectrum of PTCDI in the gas phase is shown in Fig. 6 together with the PBE simulated one. Following the same criterion adopted for perylene, we aligned the PBE simulated NEXAFS of PTCDI to the main sharp resonance of the gas phase spectrum that falls at 285.65 eV.

We observe a mismatch for the PBE simulated peak at 286.7 eV. This peak is associated with a core hole excitation localized on the imide carbon atom C7 (see next paragraphs), whose initial state

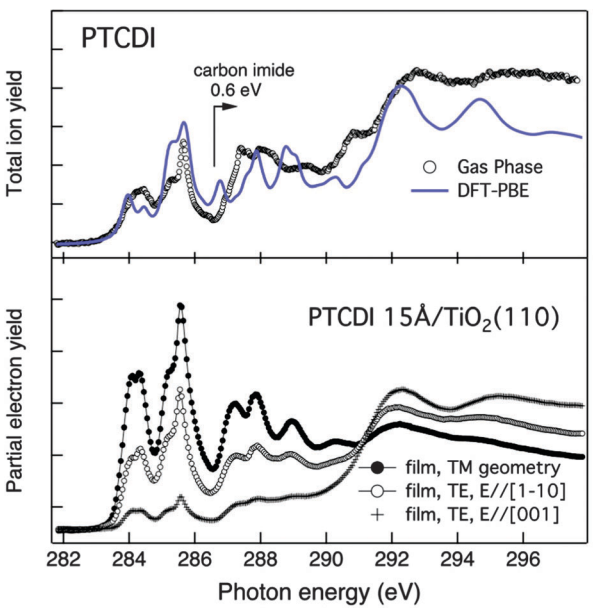

Fig. 6 PTCDI NEXAFS at the carbon K-edge. Upper panel: comparison between the gas phase NEXAFS spectrum and DFT–PBE simulation. The theoretical spectrum has been shifted by 290.70 eV, in order to match the most prominent and sharpest resonance at 285.65 eV. Lower panel: comparison between solid state spectra measured at different orientation of the surface with respect to the photon beam polarization. Experimental data are taken from ref. 32. In this case, the direct comparison of the gas and condensed phase NEXAFS requires a shift of the gas phase spectrum by −0.07 eV, which can be attributed either to the discrepancy between the different calibration procedures or to minor polarization effects due to the crystalline order of the film.

energy was underestimated by ~0.6 eV, as reported in Table 1. After correction by an energy shift of 0.6 eV, this calculated peak would perfectly match the first resonance state (~287.4 eV) of the multipeak feature experimentally observed in the 287–289 eV range. This shift is expected to affect also the higher energy molecular orbitals associated with the core hole localized on the carbon imide. We also notice that the splitting computed for the first resonance state at ~284.3 eV is smeared in the experiments, likely due to minor impurities in the PTCDI powder (see the ESI† file).

The NEXAFS spectra measured on a PTCDI multilayer (~15 Å) grown on TiO_2(110), as taken from ref. 32, for different orientations of the surface with respect to the electric field are shown in the lower panel of Fig. 6. Also in this case, the large azimuthal dichroism of the π* symmetry resonances for the spectra measured in TE geometry with different azimuthal orientations indicates that the molecules display a preferential orientation with one axis parallel to the substrate [001] direction. From the intensity ratio between the first π* resonances measured in TE (with the electric field oriented along the [1$\bar{1}$0] direction) and TM geometry, we can estimate an average tilting of PTCDI around the major axis by $\gamma \sim 40^\circ$. This value is larger than for the PTCDI monolayer because of a lower degree of order,[32] as also suggested by the occurrence of a residual intensity of the π* resonances in the spectrum measured in TE geometry when the electric field is oriented along the [001] direction. Nonetheless, PTCDI grows on a first layer that is commensurate to the substrate,[32] thus the film is expected to display a good vertical stacking of next molecular layers.

Although affected by a tilting angle larger than perylene, the NEXAFS spectra recorded in TM geometry for the PTCDI multilayer are dominated by resonance states with π* symmetry. As a consequence, we compare the TM spectrum with the PBE simulated NEXAFS along the direction *Z* normal to the molecular plane. When looking at the atomic origin of the π* resonances shown in Fig. 7, PBE calculations predict the first peak (measured at ~284.1 eV) to be contributed by transitions from three carbon atoms (C1, C2, C4), while the second peak stems solely from the C3 atom. This is at variance with the case of perylene where C4/C1 and C2/C3 are associated with the first and second peak, respectively. The LUMO near degeneracy of the ortho- (C2) and bay- (C1) carbon atoms bound to hydrogen (that are split in perylene) simply reflects the reduced CLS between them (initial-state effect). The second group of states with the main sharp peak at ~285.6 eV is associated with transitions from all the carbon atoms but the imide one (C7). As previously remarked, the first excitation associated with the imide carbon is predicted at ~286.7 eV, which, after correction by the mismatch of the PBE CLS with the experimental one (+0.6 eV), would fit the experimental resonance at ~287.2 eV (287.4 eV in the better resolved gas phase spectrum). Apart from the mismatch in the imide carbon contribution, we want to remark that the two inner carbon atoms (C3, C4), whose signal is largest in the 287–289 eV range, are predicted to display a sequence of π* symmetry states that matches quite well the observed sequence of peaks in this energy range, further strengthening our theoretical analysis.

The analysis of the symmetry and spatial distribution of the PTCDI orbitals in the presence of a localized core hole reveal

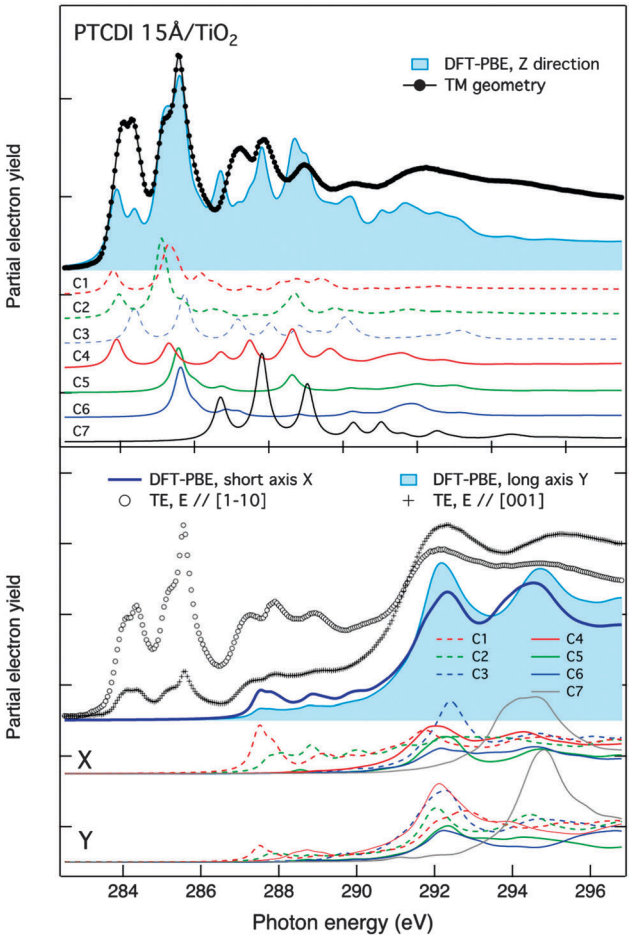

Fig. 7 Upper panel: comparison between PTCDI NEXAFS in the *z* direction (full shaded line) and an almost planar oriented thin film measured in TM geometry (open markers). Lower panel: comparison between PTCDI NEXAFS in the XY direction (shaded and full lines) and the thin film measured in TE geometry (markers) for the two opposite symmetry directions. The atomically resolved contributions (weighted by the corresponding multiplicity) to the simulated NEXAFS are shown as dashed and full lines of different colors.

some unexpected differences with respect to the perylene ones concerning the final state effects on unoccupied MOs of higher energy. Neither the energy sequence of the atom resolved contributions to the LUMO (*Z* direction only) deviates from the calculated CLS (see Fig. 8) nor the symmetry and spatial distribution of the corresponding LUMO deviate from those in the ground state (see ESI† file). In contrast, very large distortions are observed for the LUMO + 1, in particular a major contribution to the most prominent peak is predicted for the two carbon atoms C5 and C6 located on the major axis, whereas, for the ground state, these atoms are contained in the single nodal plane (perpendicular to the molecule) of the LUMO + 1. Overall, DFT calculations predict a rehybridization of the LUMO + *i* excited states larger for PTCDI than for perylene (see the ESI† file).

Finally, we analyze the σ* symmetry resonances of PTCDI, also reported in the lower panel of Fig. 7. Due to the lower degree of order of the PTCDI multilayer with respect to the

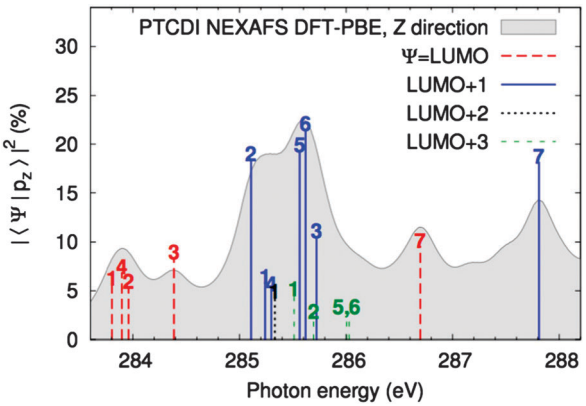

Fig. 8 The PBE calculated NEXAFS of PTCDI in the direction *Z* normal to the molecular plane (shaded curve) is shown together with vertical sticks representing the projection on the excited carbon atom $2p_z$ orbital (see numbers above the sticks for the atom species) of the various unoccupied MOs, affected by the core hole.

perylene monolayer, we experimentally observed a residual intensity from π* symmetry resonance states even when the electric field is oriented parallel to the major molecular axis (see for example the π* peaks in the 284–286 eV range). This prevents us from clearly discriminating the σ* states associated with the C–H bonds from the multiple contributions of π* symmetry states experimentally observed in the 287–288 eV range. The σ* resonances at higher energy are instead clearly identifiable and we observe an azimuthal dichroism as for perylene. The main resonance at ~292 eV is enhanced when the electric field is oriented along the [001] direction, that is along the molecular long axis *Y*. Most interestingly, an additional dichroism is observed for the second broad σ* resonance at ~295 eV. The latter resonance is not present in the NEXAFS spectra of perylene, thus being associated with the imide carbon. Both the assignment and the dichroic behavior (in energy and intensity) are correctly predicted by PBE simulations.

4 Conclusions

We have measured the NEXAFS spectra at the carbon K-edge of perylene and PTCDI both in the gas phase and in highly oriented molecular films deposited on TiO_2(110). This comparison allowed us to discriminate the different symmetry of the unoccupied molecular orbitals. Their shape and energy hierarchy result from the interplay between the different core level shifts of each carbon atom (initial state effects) and their rearrangement in the presence of the localized core hole (final state effects). We made use of *ab initio* numerical simulations in order to disentangle such initial and final state effects.

The initial state (CLS) is qualitatively well described by the PBE functional used in this work, even though the shift of the imide carbon atom of PTCDI is underestimated by 0.6 eV with respect to experiments. We have shown that calculations including a fraction of Hartree–Fock exchange mitigate such a discrepancy and yield an excellent correspondence with the measured XPS of C 1s for the carbon atoms of both perylene and PTCDI perylenic cores.

We have found a good agreement for the NEXAFS spectra of perylene, which allowed us to identify the spectral features. In particular, the σ* symmetry of the resonance at 287.1 eV is unequivocally identified and associated with specific contributions from the C–H bonds. We show that PBE calculations correctly predict the NEXAFS azimuthal dichroism of the main σ* resonance above the ionization threshold at 292.7 eV, as observed when the electric field is oriented either along the major molecular axis or along the minor one, thus allowing us to determine the full geometrical orientation by NEXAFS measurements.

In the case of PTCDI, the first two multicomponent resonances (at 284–286 eV) in the measured NEXAFS are nicely reproduced by PBE calculations, due to transitions to unoccupied MOs from the core level localized on the carbon atoms of the perylene core. The third resonance at ~287.2–287.4 eV is underestimated by 0.6 eV, similarly to the CLS of the imide carbon atom: indeed it can be associated with excitation from the 1s orbital of the imide carbon atom to the LUMO.

For both molecules, initial state effects corresponding to the calculated CLSs are reflected in the observed splitting of the first resonance, which corresponds to transitions to LUMO states. Resonances at higher energy, including LUMO + 1 and higher contributions, are largely influenced by final state effects through the distortion and energy shift of the unoccupied MOs resulting by the core–hole attraction. In conclusion, the shape and energy hierarchy of the unoccupied orbitals of perylene and PTCDI were determined in detail by exploiting the correct description of the NEXAFS resonances in our transition-potential DFT calculations with pseudopotentials and the plane-wave basis set. Such an agreement supports and extends to the case of PAHs containing hetero atoms the strength of the theoretical approach, which is best suited to the inclusion of a substrate, as relevant to the technologically important case of organic semiconductors at interfaces.

Acknowledgements

We acknowledge support from the MIUR of Italy through PRIN projects DSSCX (no. 20104XET32) and DESCARTES (no. 2010BNZ3F2). Computational resources were made available in part by CINECA (application code HP10C0TP0R).

References

1 F. S. Tautz, *Prog. Surf. Sci.*, 2007, **82**, 479–520.
2 D. R. T. Zahn, G. N. Gavrila and G. Salvan, *Chem. Rev.*, 2007, **107**, 1161–1232.
3 N. Li, K. Lee, C. K. Renshaw, X. Xiao and S. R. Forrest, *Appl. Phys. Lett.*, 2011, **98**, 053504.
4 R. Schlaf, B. Parkinson, P. Lee, K. Nebesny and N. Armstrong, *J. Phys. Chem. B*, 1999, **103**, 2984–2992.

5 S. Soubatch, R. Temirov and F. S. Tautz, *Phys. Status Solidi A*, 2008, **205**, 511–525.
6 B. A. Jones, A. Facchetti, M. R. Wasielewski and T. J. Marks, *J. Am. Chem. Soc.*, 2007, **129**, 15259–15278.
7 B. A. Jones, A. Facchetti, M. R. Wasielewski and T. J. Marks, *Adv. Funct. Mater.*, 2008, **18**, 1329–1339.
8 C. Li and H. Wonneberger, *Adv. Mater.*, 2012, **24**, 613–636.
9 C. Huang, S. Barlow and S. R. Marder, *J. Org. Chem.*, 2011, **76**, 2386–2407.
10 M. Oltean, G. Mile, M. Vidrighin, N. Leopold and V. Chis, *Phys. Chem. Chem. Phys.*, 2013, **15**, 13978–13990.
11 R. F. Fink, J. Seibt, V. Engel, M. Renz, M. Kaupp, S. Lochbrunner, H.-M. Zhao, J. Pfister, F. Wuerthner and B. Engels, *J. Am. Chem. Soc.*, 2008, **130**, 4637–4645.
12 M. Mura, X. Sun, F. Silly, H. T. Jonkman, G. A. D. Briggs, M. R. Castell and L. N. Kantorovich, *Phys. Rev. B: Condens. Matter Mater. Phys.*, 2010, **81**, 195412.
13 D. Toton, S. Godlewski, G. Goryl, J. J. Kolodziej, L. Kantorovich and M. Szymonski, *Phys. Rev. B: Condens. Matter Mater. Phys.*, 2011, **83**, 235431.
14 S. Godlewski, A. Tekiel, W. Piskorz, F. Zasada, J. S. Prauzner-Bechcicki, Z. Sojka and M. Szymonski, *ACS Nano*, 2012, **6**, 8536–8545.
15 J. Taborski, P. Vaterlein, H. Dietz, U. Zimmermann and E. Umbach, *J. Electron Spectrosc. Relat. Phenom.*, 1995, **75**, 129–147.
16 H. Oji, R. Mitsumoto, E. Ito, H. Ishii, Y. Ouchi, K. Seki, T. Yokoyama, T. Ohta and N. Kosugi, *J. Chem. Phys.*, 1998, **109**, 10409–10418.
17 U. Zimmermann, G. Schnitzler, V. Wustenhagen, N. Karl, R. Dudde, E. Koch and E. Umbach, *Mol. Cryst. Liq. Cryst.*, 2000, **339**, 231–259.
18 J. B. Simonsen, B. Handke, Z. Li and P. J. Moller, *Surf. Sci.*, 2009, **603**, 1270–1275.
19 J. Stöhr, *NEXAFS Spectroscopy*, Springer-Verlag, Berlin, 1992.
20 L. Cao, Y.-Z. Wang, T.-X. Chen, W.-H. Zhang, X.-J. Yu, K. Ibrahim, J.-O. Wang, H.-J. Qian, F.-Q. Xu, D.-C. Qi and A. T. S. Wee, *J. Chem. Phys.*, 2011, **135**, 174701.
21 A. Schöll, Y. Zou, D. Hübner, S. Urquhart, T. Schmidt, R. Fink and E. Umbach, *J. Chem. Phys.*, 2005, **123**, 044509.
22 L. Triguero, L. Pettersson and H. Agren, *Phys. Rev. B: Condens. Matter Mater. Phys.*, 1998, **58**, 8097–8110.
23 B. Gao, Z. Wu, H. Agren and Y. Luo, *J. Chem. Phys.*, 2009, **131**, 034704.
24 R. De Francesco, M. Stener and G. Fronzoni, *J. Phys. Chem. A*, 2012, **116**, 2885–2894.
25 G. Fratesi, V. Lanzilotto, L. Floreano and G. P. Brivio, *J. Phys. Chem. C*, 2013, **117**, 6632–6638.
26 M. Klues, K. Hermann and G. Witte, *J. Chem. Phys.*, 2014, **140**, 014302.
27 H. Agren, V. Carravetta, O. Vahtras and L. Pettersson, *Theor. Chem. Acc.*, 1997, **97**, 14–40.
28 C. Kolczewski, R. Puttner, O. Plashkevych, H. Agren, V. Staemmler, M. Martins, G. Snell, A. Schlachter, M. Sant'Anna, G. Kaindl and L. Pettersson, *J. Chem. Phys.*, 2001, **115**, 6426–6437.
29 M. V. Nardi, F. Detto, L. Aversa, R. Verucchi, G. Salviati, S. Iannotta and M. Casarin, *Phys. Chem. Chem. Phys.*, 2013, **15**, 12864–12881.
30 D. V. Potapenko, N. J. Choi and R. M. Osgood, *J. Phys. Chem. C*, 2010, **114**, 19419–19424.
31 V. Lanzilotto, C. Sanchez-Sanchez, G. Bavdek, D. Cvetko, M. F. Lopez, J. A. Martin-Gago and L. Floreano, *J. Phys. Chem. C*, 2011, **115**, 4664–4672.
32 V. Lanzilotto, G. Lovat, G. Otero, L. Sanchez, M. F. Lpez, J. Mndez, J. A. Martn-Gago, G. Bavdek and L. Floreano, *J. Phys. Chem. C*, 2013, **117**, 12639–12647.
33 J. B. Simonsen, *Surf. Sci.*, 2010, **604**, 1300–1309.
34 R. Blyth, R. Delaunay, M. Zitnik, J. Krempasky, R. Krempaska, J. Slezak, K. Prince, R. Richter, M. Vondracek, R. Camilloni, L. Avaldi, M. Coreno, G. Stefani, C. Furlani, M. de Simone, S. Stranges and M. Adam, *J. Electron Spectrosc. Relat. Phenom.*, 1999, **101**, 959–964.
35 G. Witte, K. Hanel, S. Sohnchen and C. Woll, *Appl. Phys. A: Mater. Sci. Process.*, 2006, **82**, 447–455.
36 P. Krüger, S. Bourgeois, B. Domenichini, H. Magnan, D. Chandesris, P. Le Fevre, A. M. Flank, J. Jupille, L. Floreano, A. Cossaro, A. Verdini and A. Morgante, *Phys. Rev. Lett.*, 2008, **100**, 055501.
37 P. Krüger, J. Jupille, S. Bourgeois, B. Domenichini, A. Verdini, L. Floreano and A. Morgante, *Phys. Rev. Lett.*, 2012, **108**, 126803.
38 S. Yu, S. Ahmadi, C. Sun, P. Palmgren, F. Hennies, M. Zuleta and M. Gothelid, *J. Phys. Chem. C*, 2010, **114**, 2315–2320.
39 M. Gothelid, S. Yu, S. Ahmadi, C. Sun and M. Zuleta, *Int. J. Photoenergy*, 2011, **2011**, 401356.
40 G. Bavdek, A. Cossaro, D. Cvetko, C. Africh, C. Blasetti, F. Esch, A. Morgante and L. Floreano, *Langmuir*, 2008, **24**, 767–772.
41 P. Giannozzi, S. Baroni, N. Bonini, M. Calandra, R. Car, C. Cavazzoni, D. Ceresoli, G. L. Chiarotti, M. Cococcioni, I. Dabo, A. Dal Corso, S. de Gironcoli, S. Fabris, G. Fratesi, R. Gebauer, U. Gerstmann, C. Gougoussis, A. Kokalj, M. Lazzeri, L. Martin-Samos, N. Marzari, F. Mauri, R. Mazzarello, S. Paolini, A. Pasquarello, L. Paulatto, C. Sbraccia, S. Scandolo, G. Sclauzero, A. P. Seitsonen, A. Smogunov, P. Umari and R. M. Wentzcovitch, *J. Phys.: Condens. Matter*, 2009, **21**, 395502.
42 J. Perdew, K. Burke and M. Ernzerhof, *Phys. Rev. Lett.*, 1996, **77**, 3865–3868.
43 E. Pehlke and M. Scheffler, *Phys. Rev. Lett.*, 1993, **71**, 2338–2341.
44 C. Adamo and V. Barone, *J. Chem. Phys.*, 1999, **110**, 6158–6170.
45 C. Gougoussis, M. Calandra, A. P. Seitsonen and F. Mauri, *Phys. Rev. B: Condens. Matter Mater. Phys.*, 2009, **80**, 075102.
46 M. Leetmaa, M. P. Ljungberg, A. Lyubartsev, A. Nilsson and L. G. M. Pettersson, *J. Electron Spectrosc. Relat. Phenom.*, 2010, **177**, 135–157.
47 G. Charlton, P. Howes, C. Nicklin, P. Steadman, J. Taylor, C. Muryn, S. Harte, J. Mercer, R. McGrath, D. Norman, T. Turner and G. Thornton, *Phys. Rev. Lett.*, 1997, **78**, 495–498.

48 R. Lindsay, A. Wander, A. Ernst, B. Montanari, G. Thornton and N. Harrison, *Phys. Rev. Lett.*, 2005, **94**, 246102.
49 M. Alagia, C. Baldacchini, M. Betti, F. Bussolotti, V. Carravetta, U. Ekstrom, C. Mariani and S. Stranges, *J. Chem. Phys.*, 2005, **122**, 124305.
50 A. Schöll, Y. Zou, M. Jung, T. Schmidt, R. Fink and E. Umbach, *J. Chem. Phys.*, 2004, **121**, 10260–10267.
51 L. N. Serkovic Loli, H. Hamoudi, J. Esteban Gayone, M. Luz Martiarena, E. A. Sanchez, O. Grizzi, L. Pasquali, S. Nannarone, B. P. Doyle, C. Dablemont and V. A. Esaulov, *J. Phys. Chem. C*, 2009, **113**, 17866–17875.
52 M. Alagia, M. Lavollee, R. Richter, U. Ekstrom, V. Carravetta, D. Stranges, B. Brunetti and S. Stranges, *Phys. Rev. A: At., Mol., Opt. Phys.*, 2007, **76**, 022509.
53 C. Nicolas and C. Miron, *J. Electron Spectrosc. Relat. Phenom.*, 2012, **185**, 267–272.
54 J. N. O'Shea, A. Saywell, G. Magnano, L. M. A. Perdigao, C. J. Satterley, P. H. Beton and V. R. Dhanak, *Surf. Sci.*, 2009, **603**, 3094–3098.

